Hindawi Publishing Corporation
International Journal of Rotating Machinery
Volume 2012, Article ID 601837, 10 pages
doi:10.1155/2012/601837

*Research Article*

# Deterioration of Thermal Barrier Coated Turbine Blades by Erosion

**Rohan Swar,[1] Awatef Hamed,[1] Dongyun Shin,[1] Nathanial Woggon,[1] and Robert Miller[2]**

[1] *School of Aerospace Systems, University of Cincinnati, 2600 Clifton Avenue, Cincinnati, OH 45221, USA*
[2] *NASA John H. Glenn Research Center, Cleveland, OH 44135, USA*

Correspondence should be addressed to Dongyun Shin, shindn@mail.uc.edu

Received 21 June 2012; Revised 10 October 2012; Accepted 12 October 2012

Academic Editor: J.-C. Han



A combined experimental and computational study was conducted to investigate the erosion of thermal barrier coated (TBC) blade surfaces by alumina particles ingestion in a single-stage turbine. In the experimental investigation, tests were performed to determine the erosion rates and particle restitution characteristics under different impact conditions. The experimental results show that the erosion rates increase with increased impingement angle, impact velocity, and temperature. In the computational simulations, an Euler-Lagrangian two-stage approach is used in obtaining numerical solutions to the three-dimensional compressible Reynolds-Averaged Navier-Stokes equations and the particles equations of motion in each blade passage reference frame. User defined functions (UDFs) were developed to represent experimentally based correlations for particle surface interaction models and TBC erosion rates models. UDFs were employed in the three-dimensional particle trajectory simulations to determine the particle rebound characteristics and TBC erosion rates on the blade surfaces. Computational results are presented in a commercial turbine and a NASA-designed automotive turbine. The similarities between the erosion patterns in the two turbines are discussed for uniform particle ingestion and for particle ingestion concentrated in the inner and outer 5% of the stator blade span to represent the flow cooling of the combustor liner.

## 1. Introduction

Turbomachinery erosion presents a challenging problem when gas turbine engines operate in dusty environments [1–3]. Some of the mechanisms that cause particle ingestion are (a) the vortex from engine inlet-to-ground during high-power setting with the aircraft standing or moving on the runway; (b) storms transporting sand to several thousand feet altitude; (c) thrust reverser afflux at low airplane speed blowing sand, ice, and other particles into the engine inlets. Erosive solid particles may also be produced during the combustion process, from the burning of different types of heavy oils or synthetic fuels. Helicopter engines are especially susceptible to large amounts of dust and sand ingestion during hover, takeoff, and landing.

It is very difficult to remove all solid particles from the gas stream without taxing the performance of gas turbine engines [4, 5]. Even small particles of one to thirty micron sizes have been known to be very damaging to the exposed components of coal burning turbines [6]. In turbomachinery, particle impacts are known to increase tip clearances and blade surface roughness and produce changes in the blade leading and trailing edges [7]. Because TBC erosion is detrimental to the thermal protection of turbine blades, it has been identified as a life-limiting factor for gas turbines [8–10]. With the increasing use of thermal barrier technology to protect highly loaded and rotating turbine components [11], further studies are needed to support thermal protection for life extension.

Different process combinations such as cutting, fatigue, brittle fracture, and melting mechanisms have been proposed to govern material removal by erosion. According to experimental studies of blade alloys and coating materials, their erosion rates are influenced by particle impact velocities and impingement angles and by the operating temperatures [3]. Experimental characterization of material erosion resistance requires special facilities that control particle-laden flow around the sample to achieve the desired impact

conditions over the tested samples [12]. Prior TBC erosion test results have demonstrated that electron beam-physical vapor deposited (EB-PVD) TBC erosion rates are an order of magnitude less than plasma sprayed (PS) TBC and that both increase linearly with particles impact velocity [13, 14]. Experimental studies of particle surface impacts are also necessary to provide particle rebound characteristics over the range of impinging conditions encountered in turbomachines [3, 7].

Blade erosion in turbomachines is affected by rotational speed and flow conditions, blade geometry and blade row location, blade material, and particle characteristics [3, 7]. Under two-phase flow conditions, the gas and particles experience different degrees of turning through the blade passages. Deviation from the gas flow path increases with particle inertia causing repeated impacts with the various surfaces. Surface impacts alter the direction and velocity of the particles as well as their distribution through subsequent stages. Experimental studies that simulate erosive particle impact conditions in the engine environment are essential to blade and coating material development. The associated blade surfaces erosion requires knowledge of the particle three-dimensional trajectories and their impact statistics on the various engine surfaces in addition to surface material erosion behavior under the impact conditions.

Trajectory simulations are based on the numerical integration of the particles' equations of motion through the successive turbomachinery stationary and rotating blade rows. The simulations require the 3D flow field and blade passage geometries as inputs and a model for particle restitution conditions following each surface impact. The basis for particle trajectory simulations in turbomachines continues to be Eulerian-Lagrangian with one way coupling between the particles and flow [15, 16]. Currently three-dimensional flow field solutions of the Reynolds averaged Navier-Stokes equations for turbulent flow through the blade passages [16] are used in turbomachinery trajectory simulations.

Hamed and Tabakoff [17] developed a methodology to predict turbomachinery blade surface erosion using blade surface statistical impact data computed from particle trajectory simulations and correlations based on blade material erosion test results. It was used in the prediction of blade erosion in both axial and radial compressors and turbines [3] and erosion of turbine blade coating developed for automotive and ground based gas turbine applications.

In the current work, a combined experimental and numerical investigation was conducted to study the deterioration of thermal barrier coating on turbine blades by erosive particles. Experimental measurements were obtained for EB-PVD 7YSZ-coated INCO718 coupons in the high-temperature erosion tunnel under different impact conditions by alumina particles. Measurements were also obtained for particle restitution characteristics at different impact angles relative to the coated sample using Particle Image Displacement Velocimetry (PIDV). The experimental measurements of surface erosion and particle restitution were used to develop empirical erosion and restitution models. The numerical simulations for the three-dimensional flow field and particle trajectories were combined with experimentally based surface interaction models to predict TBC erosion over the stator and rotor blade surfaces in a single-stage commercial gas turbine and in a NASA automotive turbine design. Both the TBC coated blade erosion patterns and the locations of maximum erosion were found to be similar. The three-dimensional particle trajectories are presented through the NASA-designed turbine blade passages to characterize the mechanisms producing these erosion patterns. The blade surface areas subjected to repeated impacts at the highest particle velocities are shown to coincide with the locations of maximum TBC erosion rates.

## 2. Experimental Work

Erosion tests were carried out for 25.4 mm × 25.4 mm × 1.5875 mm (1″ × 1″ × 1/16″) INCO718 coupons coated with EB-PVD 7YSZ over a range of impact conditions by different size alumina particles. The coupons were mounted on a sample holder and placed at the designated angles in the high-temperature erosion wind tunnel shown schematically in Figure 1 and subjected to erosion by a calibrated mass of particles. The holder protected all but one target coupon surface that was exposed to particle impacts. The samples were weighed before and after the erosion tests to determine the weight loss due to erosion by the impacting particles.

The University of Cincinnati (UC) erosion wind tunnel [12] shown schematically in Figure 1 consists of the following components: particle feeder (A), main air supply pipe (B), combustor (C), particle pre-heater (D), particle injector (E), acceleration tunnel (F), test section (G) and exhaust tank (H). Abrasive particles of a given constituency and measured weight are placed into the particle feeder (A). The particles are fed into a secondary air source and blown into the particle preheater (D) and then to the injector (E), where they mix with the primary air supply (B), which is heated by the combustor (C). The particles are then accelerated via high-velocity air in a constant-area steam-cooled duct (F) and impact the specimen in the test section (G). The particulate flow is then mixed with coolant and directed to the exhaust tank. As can be seen from Figure 1, the tunnel geometry is uninterrupted from the acceleration tunnel throughout the test section in order to preserve the aerodynamics of the flow passing over the samples. Particles' impact velocities are calibrated with the tunnel air flow, while the particle impingement angle is controlled through the sample orientation. A measured mass of particles is fed into the flow after the test sample reaches equilibrium temperature.

The erosion rate, $\varepsilon$ in mg/g is defined as the ratio of the measured coated sample erosion mass loss, $\Delta W$, to the mass of erosive particles impacting surface, $Q_p$, which is determined from the tunnel calibration according to the sample size and impingement angle [18]:

$$\varepsilon = \frac{\Delta W}{Q_p}. \tag{1}$$

Particle restitution characteristics after impacting the coated coupons were measured in a second tunnel equipped with

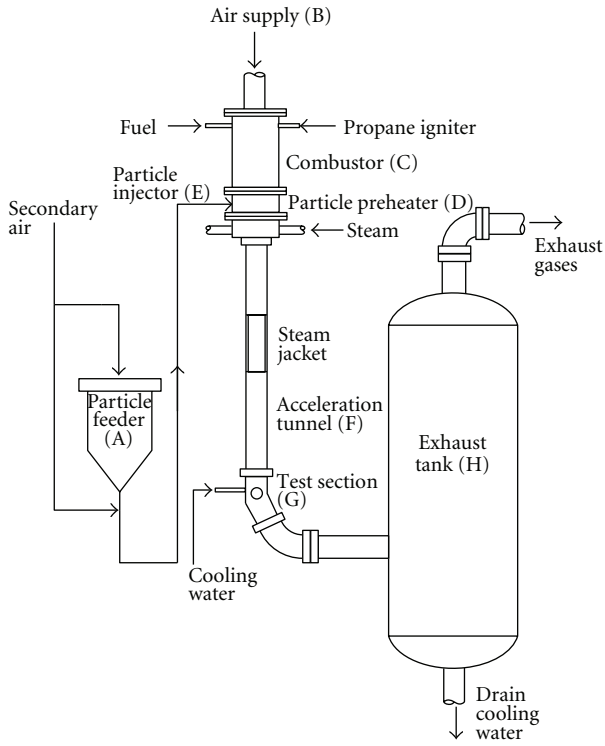


Figure 1: Schematic of erosion test facility.

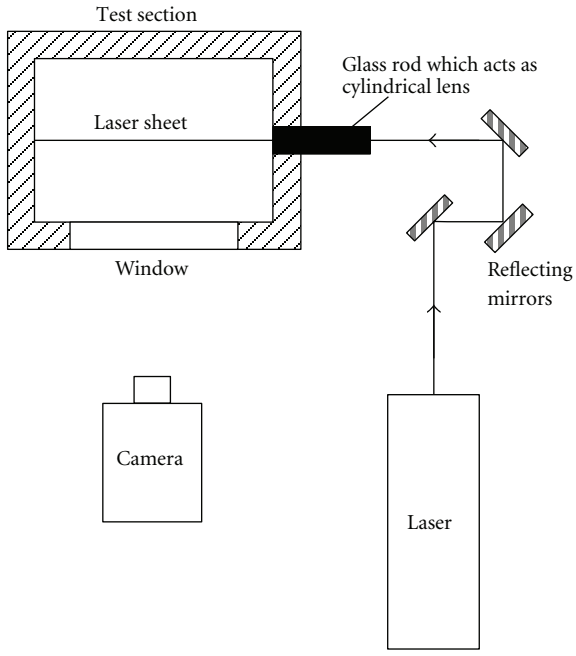


Figure 2: Test section, laser Sheet and camera.

optical window in the test section for recording particle trajectories using high-speed photographic methods at room temperature. A Phantom high-speed digital camera (model V 9.1) with a Nikon lens was used to photograph the particle trajectories. The camera had a maximum frame speed of 50,000 fps, but a frame rate of 27,000 frames per second (37 $\mu$s interval) and 256×256 resolution were appropriate for the light intensity obtained from a 250 mW Spectra-Physics laser source (454–676 nm wavelength). Referring to Figure 2, the laser sheet was 1.65 mm thick and 50 mm in height at the frame of interest and the exposure time could be set as low as 3 $\mu$s. The camera was connected to a computer and its graphical user interface (GUI) software was used to set the frame speed and resolution, after it was focused on a reference point in the laser sheet before recording the images.

The magnitude and direction of the particle impact and rebound velocities were measured in the plane of the laser sheet. The $x$ and $y$ coordinates of a particle in each frame were determined using Phantom Cine Viewer image processing software. By comparing successive images, the trajectory of the particle was calculated using Particle Image Displacement Velocimetry (PIDV) technique [19–21]. The image of a 25.4 mm mark was used as a reference length to provide the actual distance the particle traveled between successive frames as shown in Figure 3. The particle velocity, $V$, was calculated based on the time between two successive frames:

$$V = \frac{\delta S}{\delta t} = \frac{FRd}{r}, \tag{2}$$

where $\delta t$ = time between successive frames, sec, $F$ = number of frames per second, $V$ = particle velocity, $\delta S$ = actual distance traveled by particle between two consecutive frames, $R$ = actual length of the reference mark in the test section, $d$ = distance traveled by particle as obtained from the pixel count, $r$ = length of the reference mark as obtained from the pixel count.

The velocity and directional restitution coefficients were determined from three successive frames of interest in order to exclude the postimpact influence of the tunnel flow on the rebounding particle trajectory. Error estimations of the results obtained from high-speed photography were carried out using the $t$-distribution method [21] with 95% confidence interval.

## 3. Computational Work

Numerical simulations were conducted using ANSYS CFX 12 [22] to calculate the three-dimensional flow field and the associated 26 micron particle trajectories in a single-stage gas-turbine. The Eulerian-Lagrangian two stages, one-way particle interaction model approach was used because of the typically low particle concentration in gas turbines.

Pointwise V16 [23] code was used to generate the structured computational grids in the stator and rotor blade passages of the single-stage turbine. Its elliptic solver was used to improve the grid quality especially in the high turning rotor blade passage. Figure 4 shows the three-dimensional H-O computational grids used in the NASA-designed turbine flow field and particle dynamics simulations. Grid size was based on our prior experience in large commercial engines [16]. The grids were clustered near the blade passage surfaces to achieve the $y+ < 3$ at the first grid point next to the surface.

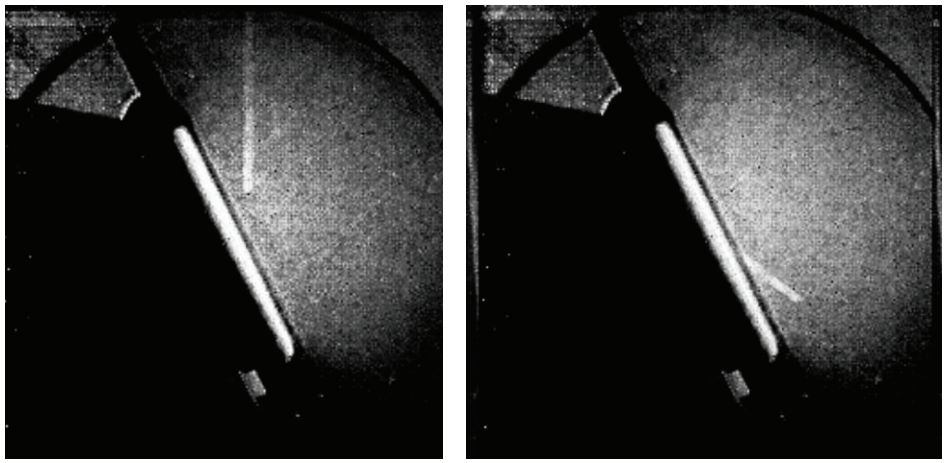

(a) (b)

Figure 3: High-speed photography images.

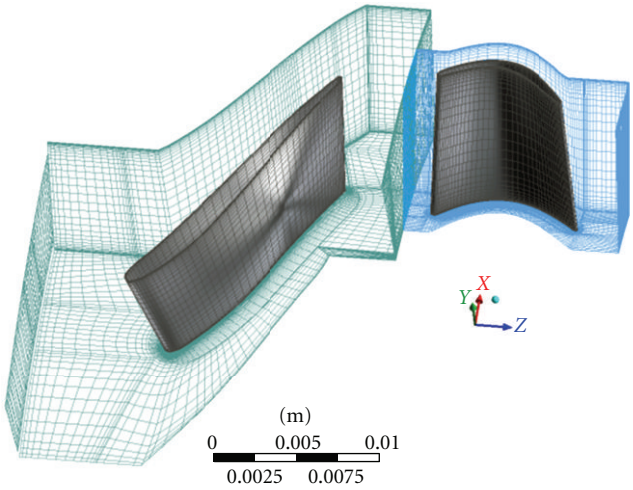


Figure 4: Computational grids of the NASA-designed turbine.

The three-dimensional flow field solution was obtained for the compressible Reynolds averaged Navier-Stokes equations in conservation form and the $k$-$\omega$ based Shear-Stress-Transport (SST) model. Advection fluxes were evaluated using the high-resolution scheme in ANSYS CFX 12 [22] which is second-order accurate with convergence criteria of $10^{-5}$ RMS residual. Because of the very-high particle velocities in the turbine particularly after rebounding from rotor blade surface impacts, the turbulence stochastic effects are negligible and the aerodynamic forces on the particles are dominated by drag due to particle slip velocities relative to the gas velocities.

The total pressure, total temperature inlet and flow direction were specified at the inlet boundary and uniform averaged static pressure was specified at the outlet boundary with the periodic interface boundary conditions invoked in the stator and rotor blade passages. A mixing plane model was used at the stator-rotor interface. The simulations were conducted for particles entering the turbine in the same direction as the inlet gas flow but with 50% the value of the inlet gas velocities.

The nominally 26 micron erosive alumina particles were assumed to be ingested at the same temperature as the gas inflow. Convective heat transfer coefficient based on ANSYS CFX 12 [22] correlation represented the interphase energy exchange. Particle trajectories were computed using forward integration and taking into consideration the momentum and heat exchange with the flow field based on the three-dimensional flow solution. The particle-tracking integration time step was chosen locally as the element length scale divided by the particle speed divided by the 100 integration steps per element [22].

Particle surface interaction modeling was based on experimental data obtained for TBC coated samples over a range of impact conditions by the alumina particles. The restitution and erosion prediction empirical models were implemented in ANSYS CFX 12 [22] as user-defined functions.

## 4. Results and Discussions

*4.1. Experimental Results.* Figure 5 presents sample results for the experimentally measured erosion rates variation with particle impingement angles for 10 mil EB-PVD 7YSZ coated INCO718 samples and for samples of the INCO 718 substrate at 1093°C (2000°F) temperature and 365.8 m/s (1200 ft/s) impact velocity. The maximum erosion rate for the EB-PVD TBC coating occurred at 90° impingement angle while that for INCO substrate occurred between 20°–30° which are typical brittle and ductile materials erosion behavior respectively. One can see from Figure 6(a) that the nominally 26 $\mu$m, mass mean erosive alumina particles have angular shapes with sharp corners. The particles size distribution is shown in Figure 6(b).

Figures 7 and 8 present experimental results for EB-PVD TBC erosion rates variation with impingement angles at

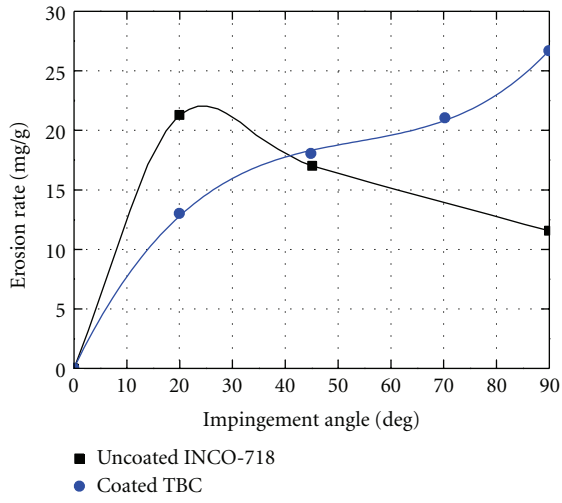


Figure 5: Measured erosion rates due to 26 $\mu$m alumina particles on TBC-coated and uncoated samples ($T$ = 1093°C (2000°F), $V$= 365.8 m/s (1200 ft/s)).

982°C (1800°F), and 871°C (1600°F), respectively. According to these results the erosion rates increase with temperatures and with particle impact velocities at all impingement angles. This is consistent with the TBC erosion test results presented at 90° impact angle in prior investigations by Tabakoff [13] and Nicholls et al. [14]. The following experimentally based TBC erosion rate correlations were implemented in the UDF and used in ANSYS CFX 12 [22] to compute the TBC erosion rates on the blade surfaces:

$$\varepsilon = \left(1.293\beta_1 - 1.301\beta_1^2 + 0.473\beta_1^3\right)(3.28V_1)^n,$$
$$n = 0.0584 + 0.000476T, \tag{3}$$

where $\beta_1$ = particle impingement angle, radians, $V_1$ = particle impact velocity, m/s, $n$ = velocity exponent, $T$ = test temperature, °C.

Several post erosion tested samples were examined using Scanning Electron Microscope to investigate posterosion particle deposition. Sample results are presented in Figure 9 for pre- and posterosion test samples. Particle deposition was rarely observed on the posterosion test samples, as shown in the posterosion ×1000 magnification image.

The experimental results were used to derive the particle velocity and angle restitution coefficients $e_V$ and $e_\beta$ as a function of the particles impingement angle $\beta_1$:

$$e_V = \frac{V_2}{V_1} = 0.5 + 1.9369\beta_1 - 4.0075\beta_1^2 + 3.1881\beta_1^3 - 0.8218\beta_1^4,$$
$$e_\beta = \frac{\beta_2}{\beta_1} = 0.9832 + 0.474\beta_1 - 3.5837\beta_1^2 + 3.4188\beta_1^3 - 0.9569\beta_1^4, \tag{4}$$

where $\beta_1$ = particle impingement angle, radians.

Table 1: NASA-designed automotive turbine (TMX-71717) blade geometry.

| Blade row | Stator | Rotor |
|---|---|---|
| Pitch (cm) | 2.096 | 0.5621 |
| Mean chord (cm) | 2.311 | 1.043 |
| Height (cm) | 1.118 | 1.105 |
| L.E. radius (cm) | 0.0635 | 0.0331 |
| T.E. radius (cm) | 0.0191 | 0.0191 |
| Number of blades | 15 | 56 |

Table 2: Operating conditions for NASA-designed turbine.

| Parameters | NASA 1979 design automotive turbine TMX-71717 |
|---|---|
| Inlet total temperature | 1325 (K) |
| Inlet total pressure | 3.92 (atm) |
| Mass flow rate | 0.598 (kg/s) |
| Rotor speed | 6126.9 (rad/s) |
| Shaft power | 22.615 (kW) |
| Reaction | 0.8013 |
| Total-to-total polytrophic efficiency % | 78.5385 |

However, ANSYS CFX 12 [22] requires user-defined functions in the form of restitution coefficients that are normal and tangential to the impacted surface. The experimental correlations of (4) were therefore used to compute the normal and tangential restitution coefficients $e_n$ and $e_t$ that are presented in Figure 10 using the following equations:

$$e_n = e_V \frac{\mathrm{Sin}\left(\beta_1 e_\beta\right)}{\mathrm{Sin}\left(\beta_1\right)},$$
$$e_t = e_V \frac{\mathrm{Cos}\left(\beta_1 e_\beta\right)}{\mathrm{Cos}\left(\beta_1\right)}. \tag{5}$$

*4.2. Computational Results.* Numerical simulations for the three-dimensional flow field, particle trajectories, and TBC blade-coating erosion were conducted for a single-stage commercial turbine and for a NASA-designed automotive turbine whose geometry and operational characteristics are in the public domain as listed in Tables 1 and 2. The two turbines have comparable inlet gas temperatures in spite of the commercial turbine's higher shaft power.

Mach number carpet plots at 50% blade span for the commercial turbine and the NASA designed turbine are presented in Figure 11. The Mach number contours in the reference frame of each blade row indicate slightly higher values in the NASA designed turbine blade passages.

Sample results of the predicted TBC erosion rates per unit mass of ingested particles into the two turbines are presented in Figures 12 through 15 for uniform particle loading then for particle ingestion localized in the combustor cooling flow near both the inner and outer 5% of the span.

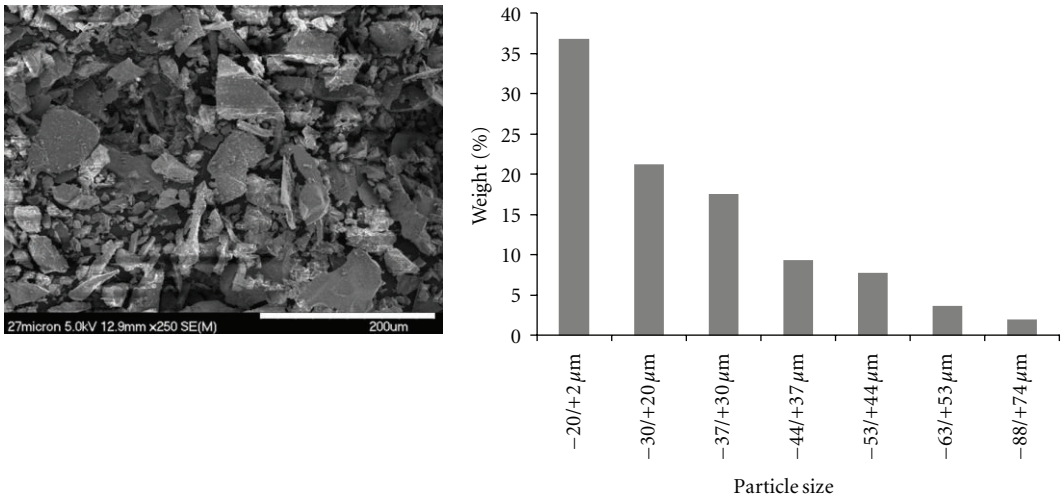


(a) Scanning electron microscope image of sample particles

(b) Particle size ($\mu$m) versus percent by weight

FIGURE 6: Nominally 26 $\mu$m alumina particles.

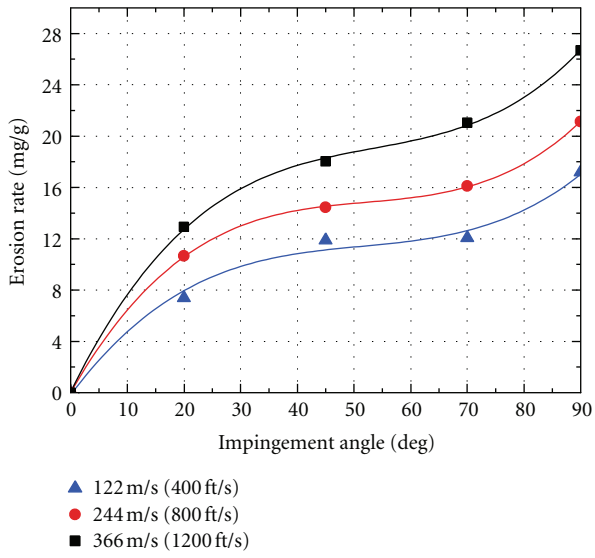


FIGURE 7: TBC erosion rates by 26 $\mu$m alumina particles at 982°C (1800°F).

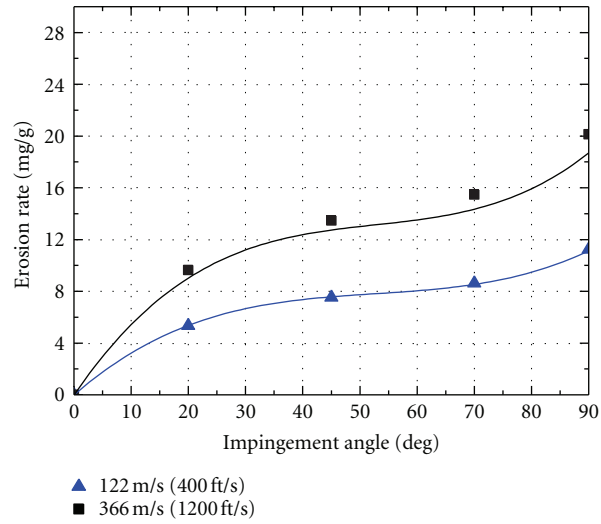


FIGURE 8: TBC erosion rates by 26 $\mu$m alumina particles at 871°C (1600°F).

Figure 12 shows the predicted thermal barrier coating erosion rates on the commercial turbine's stator and rotor blade surfaces. The figure indicates relatively low erosion rates of the thermal barrier coating on the pressure side of the stator blade leading edge. Regions of high TBC can be seen on the stator and rotor blade suction sides. The high TBC erosion rates are mainly closed to the outer radius towards the trailing edge of the stator suction surface and the leading edge of the rotor suction surface.

Figure 13 shows the computed thermal barrier coating erosion rates on the commercial turbine's stator and rotor blade surfaces when the particle seeding is only within 5% of the span near the hub and shroud. The TBC erosion on the stator suction side is seen to occur almost exclusively along these thin bands. The highest erosion rates are at the casing towards the trailing edge of the stator blade suction side and at the shroud towards the leading edge of the rotor blade suction side as in the previous results for uniform particle ingestion. However, a region of TBC erosion can be seen at the tip of the aft part of the stator pressure surface. This is typically attributed to the impacts by the high-inertia particles continuing their axial ingestion velocity into the stator blade passage.

Figures 14 and 15 present the computed thermal barrier coating erosion rates on the NASA designed turbine stator and rotor blade surfaces for uniform particle seeding (Figure 14) and for particle seeding within 5% of the span

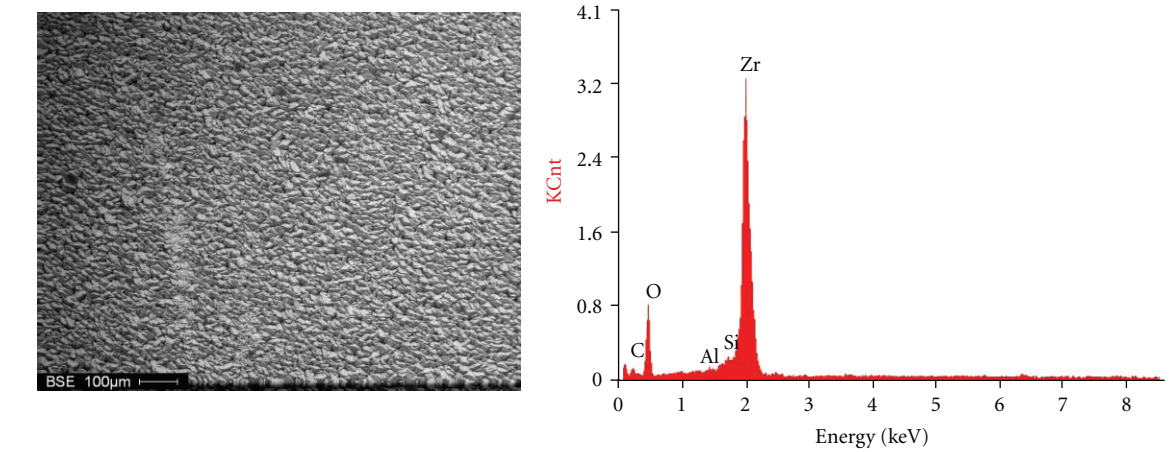


(a) Preerosion test (×100 magnification)

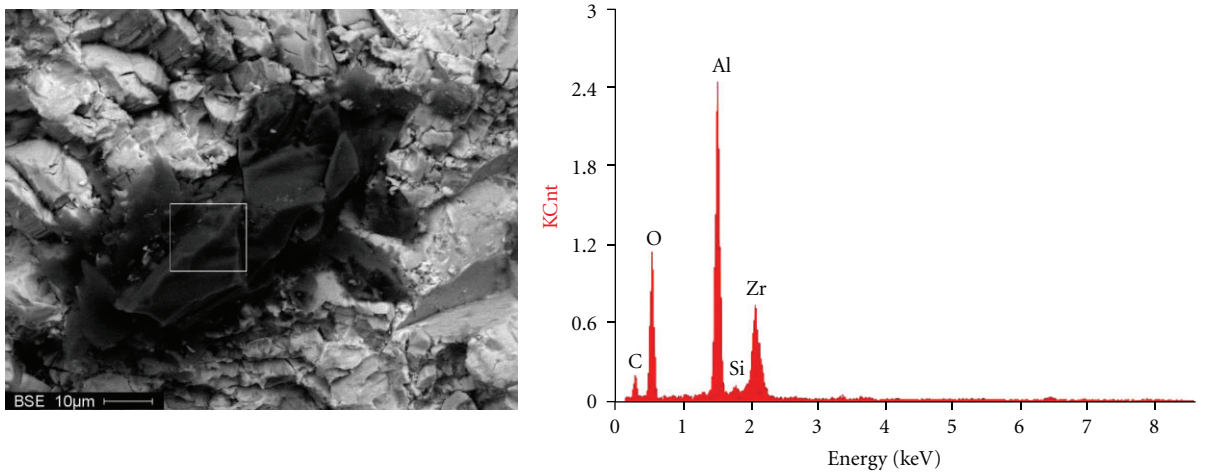


(b) Posterosion test (×1000 magnification)

Figure 9: Sample TBC surface scans with electron microscope.

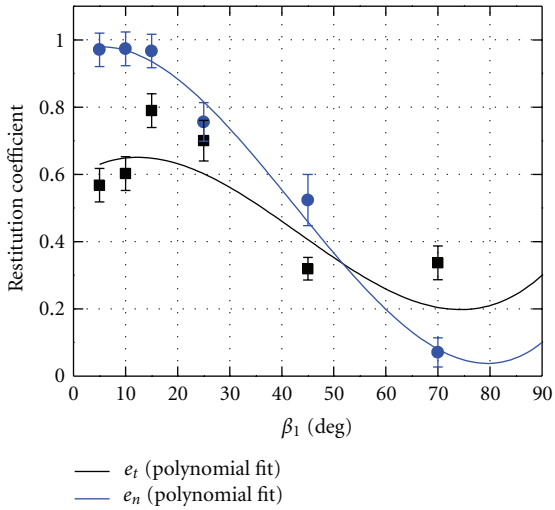


Figure 10: Tangential and normal restitution coefficients variation with impact angles.

near the hub and shroud (Figure 15). In both cases, the highest erosion rates are seen to occur on rotor blades suction surface at the shroud close to the leading edge and on the stator blades suction surface at the casing near trailing edge. These patterns are similar to those predicted in the case of commercial turbine (Figures 12 and 13). A region of very low TBC erosion rates is seen at the outer radius on the stator pressure side. Referring to Figure 11, these can be seen to be associated with the lower turning angles in the NASA-designed turbine stator compared to the commercial turbine where the high-inertia particles impacted the stator pressure surface. In the case of particle seeding within 5% of stator blade span (Figure 15), lower erosion rates are seen over regions of the stator pressure side and rotor suction side that trace the particle-ingested near the inner radius.

Figure 16 shows 25 sample trajectories with color contouring of their velocity magnitude for 26 micron alumina particles in the NASA designed turbine corresponding to particle seeding within 5% of the span near the hub and shroud. Particles are seen to enter at the stator and for the

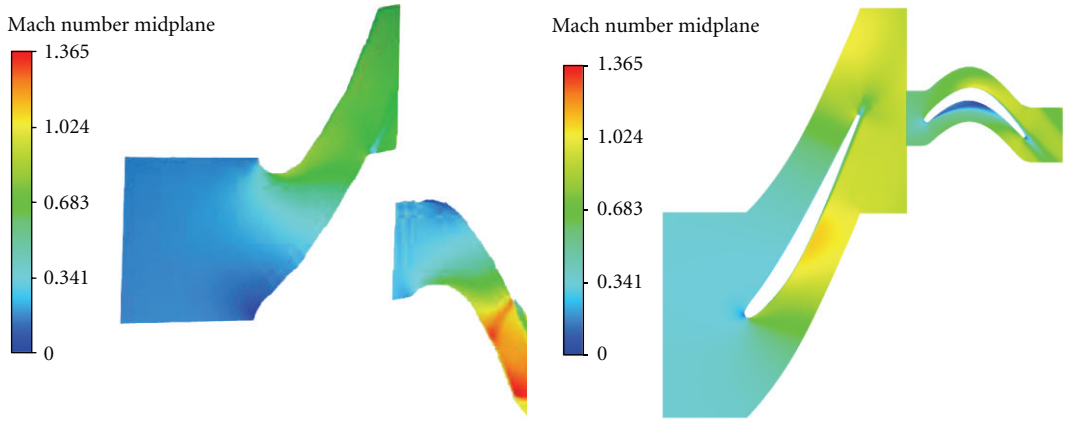


(a) Commercial turbine (b) NASA-designed turbine

Figure 11: Mach number contours at the 50% blade span.

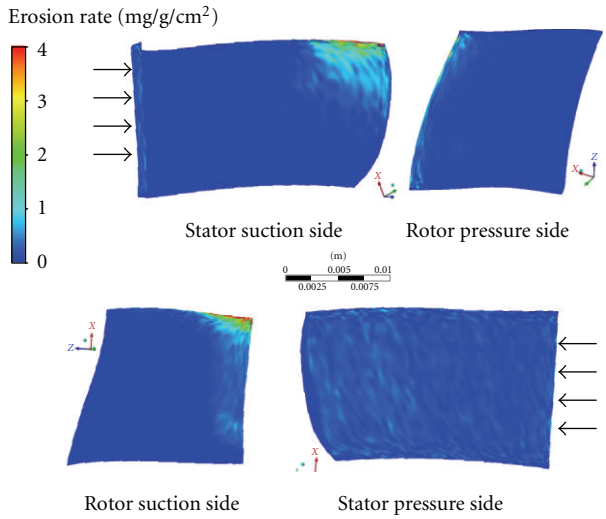


Figure 12: TBC erosion rates on blade surfaces in the commercial turbine for uniform particle loading at 50% of the gas velocity.

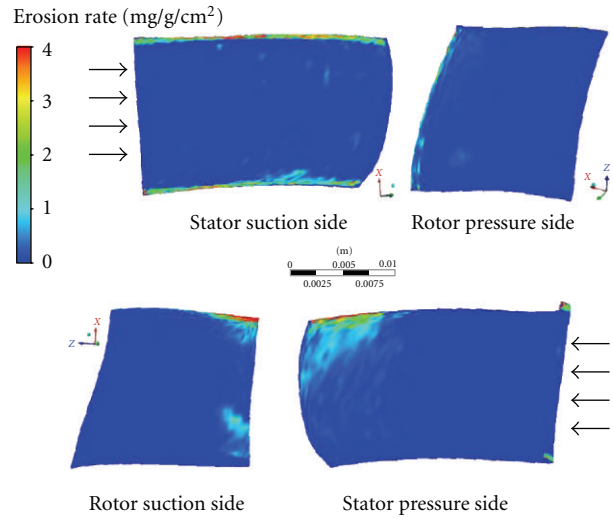


Figure 13: TBC erosion rates on blade surfaces in the commercial turbine for particles seeding within 5% of stator blade span near the hub and shroud at 50% of the gas velocity.

most particles continue along their path through the stator blade passages with negligible interactions with the blade surfaces. However as they enter the rotor blade passages, they impact the rotor blades suction side towards the leading edge. The particles rebound with high circumferential velocities after their rotor blade suction surface impacts, which immediately drives them radially outward and back into the stator blade passages.

Figure 17 is a schematic showing the cause of particle impacts occurring towards the leading edge of the rotor blade suction surfaces. According to the relative and absolute velocity vectors in Figure 17, that happens when the particles leave the stator blade row with lower absolute velocities than the gas either because of their lower ingestion velocity or because of the momentum loss associated with the stator pressure side impacts. The particles are seen to enter the rotor blade passages with negative incidence angle in the rotating frame of reference and hence they impact the rotor suction surfaces. These particles rebound from the rotor blades suction surfaces near the leading edge with very high velocities in the absolute reference frame. That causes their centrifugation in radially outward direction as they reenter the stator blade passage and impact its suction surface near the trailing edge. Several of the particles repeat this impact pattern and hence this phenomenon dominates the TBC erosion rates on the blade surfaces as shown previously in Figures 12 through 15. The particles eventually continue their trajectories through the rotor's high-turning blade passages and impact both pressure and suction surfaces of the rotor blades. However their impacts cause minor TBC erosion rates because their low-impact velocities relative to the rotor blades.

Table 3 lists the corresponding local maximum TBC erosion rates in each case as well as the computed overall TBC erosion rates in the stator and rotor blades. Comparable

Table 3: Computed overall blades and maximum local TBC erosion rates on the commercial turbine and the NASA-designed turbine.

| Turbine | Particle radial loading % span | Maximum local erosion rate (mg/g/cm$^2$) | Overall blade erosion rate (mg/g) | |
|---|---|---|---|---|
| | | | Stator | Rotor |
| Commercial turbine | 5% | 72.94 (Rotor suction side) | 0.78 | 0.93 |
| | 100% | 31.16 (Stator suction side) | 0.83 | 0.87 |
| NASA turbine | 5% | 60.21 (Stator suction side) | 1.50 | 0.88 |
| | 100% | 20.43 (Stator suction side) | 0.89 | 0.73 |

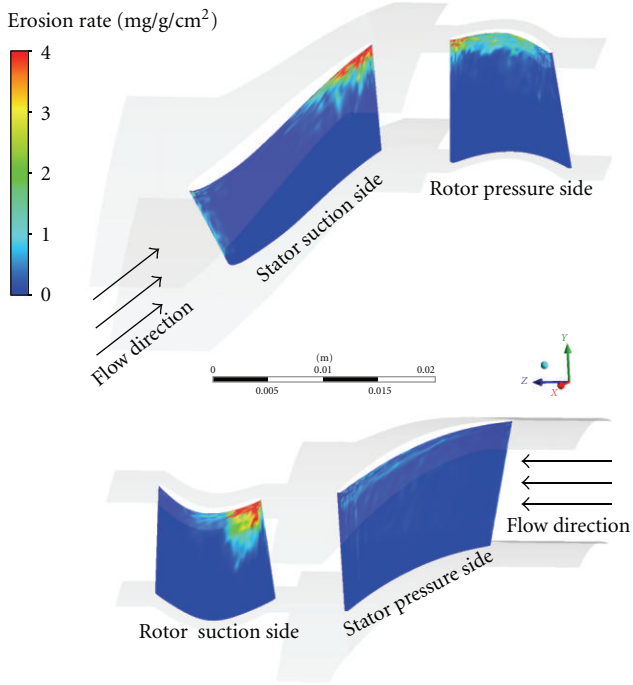


Figure 14: TBC erosion rates on blade surfaces in the NASA-designed turbine for uniform particle loading at 50% of the gas velocity.

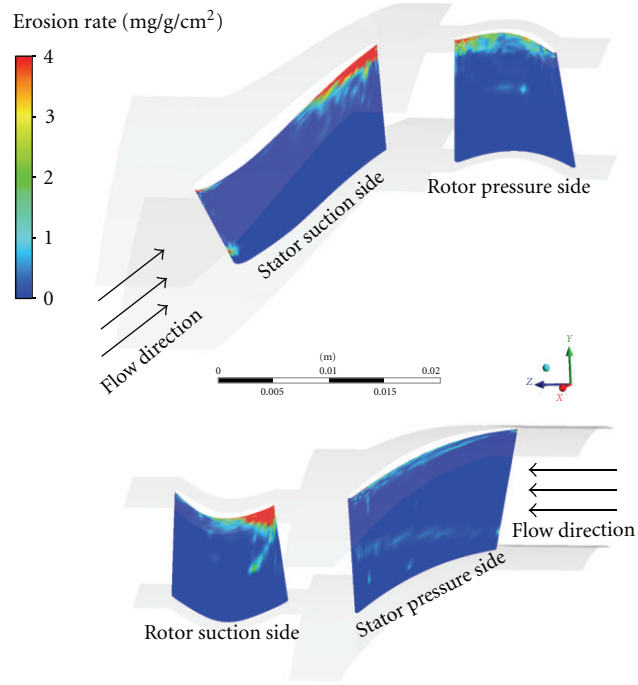


Figure 15: TBC erosion rates on blade surfaces in the NASA-designed turbine for particles seeding within 5% of stator blade span near the hub and shroud at 50% of the gas velocity.

erosion rates are predicted in the two turbines with the exception of the higher overall stator blade TBC erosion in the NASA designed turbine. Comparing Figures 13 and 15 one can observe larger area of high TBC erosion rates on the stator suction side of the NASA-designed turbine. This can be attributed to a higher percentage of the ingested particles rebounding from the high-solidity blades in the NASA-designed turbine. Referring to Table 1, the stator blade pitch is 3.8 times the rotor pitch in the NASA-designed turbine. On the other hand, the stator blade pitch is only 1.45 times the rotor blade pitch in the commercial turbine. Otherwise, similar erosion patterns in the two turbines are associated with the particle trajectories' high absolute rebound velocities from the rotor suction surface impacts.

## 5. Conclusions

A combined experimental and computational study was performed to investigate TBC deterioration on turbine stator and rotor blade surfaces due to erosion by solid particle impacts. Erosion tests were conducted for INCO718 coupons coated with 10 mils nominal of 7YSZ EB-PVD TBC over a range of impact conditions by 26 micron alumina particles. Experimental results are presented for the measured TBC coating and substrate erosion rates and for the alumina particle restitution after impacting the TBC-coated samples. The measurements indicate that the EB-PVD TBC erosion rates increase with the impingement angle, impact velocity, and temperature. The normal and tangential velocity restitution coefficients were found to decrease with increasing impact angle. Experimental-based correlations were derived and implemented in User-defined functions which were then used in the particle trajectory simulations and blade TBC erosion predictions.

The three-dimensional computational results in a single-stage commercial and NASA-designed compressor drive turbine indicate that the erosion patterns were similar in the two turbines with high TBC erosion rates at the casing towards the trailing edge of the stator blade suction side and at the shroud towards the leading edge of the rotor

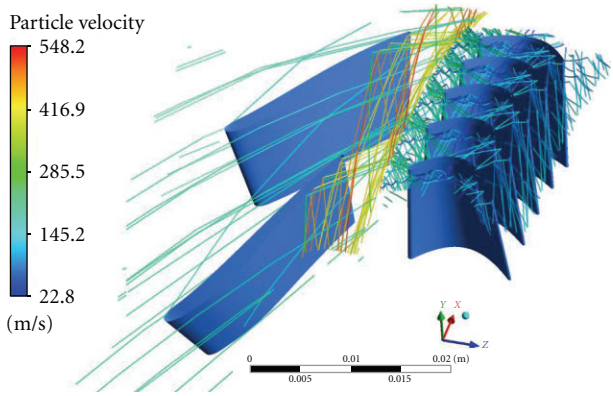


Figure 16: Sample particle trajectories including radial projection for particles seeding within 5% of stator blade span near the hub and shroud at 50% of the gas velocity in the NASA-designed turbine.

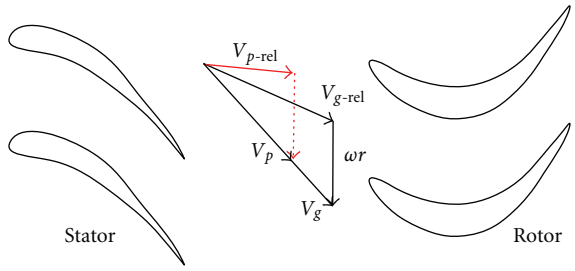


Figure 17: Schematic showing effect of particle slip velocity at the stator exit on entrance condition in the rotor reference frame.

blade suction side. The predicted three-dimensional particle trajectories through the NASA designed turbine indicate that the high erosion rates result from the negative incoming incidence angles of the particles in the rotor reference frame that causes them to impact the rotor suction surface near the leading edge and their subsequent high absolute rebounding velocities they acquire from these impacts. Subsequently the particles bounce back into the stator blade row passage and impact the stator blade suction surface near the trailing edge.

## Acknowledgments

This work was sponsored by NASA under Contract NNX07AC69A. The authors also would like to thank Dr. Widen Tabakoff for his support and suggestions in this study.

## References

[1] R. C. Sirs, "The operation of gas turbine engines in hot and sandy conditions-royal air force experiences in the gulf war," Tech. Rep. AGARD-CP-558, paper no. 2, 1994.

[2] H. J. Mitchell and F. R. Gilmore, "Dust-cloud effects on aircraft engines: emerging issues and new damage mechanisms," RDA-TR-120012-001, 1982.

[3] A. Hamed, W. Tabakoff, and R. Wenglarz, "Erosion and deposition in turbomachinery," *Journal of Propulsion and Power*, vol. 22, no. 2, pp. 350–360, 2006.

[4] M. G. Mund and H. Guhna, "Gas turbine dust air cleaners," Tech. Rep. ASME Paper 70-GT-104, 1970.

[5] D. L. Mann and G. D. Wares, "Future direction in helicopter engine protection system configuration," Tech. Rep. AGARD-CP-588, paper no. 4., 1994.

[6] L. McCoy, "The coal burning gas turbine project," Report of the Interdepartmental Gas Turbine Steering Committee, Australian Government Publishing Service, 1973.

[7] A. Hamed, W. Tabakoff, and R. Wenglarz, *Particulate Flow and Blade Erosion*, Von Karman Institute for Fluid Dynamics Lecture Series 1988-08, 1980.

[8] S. M. Meier and D. K. Gupta, "Evolution of thermal barrier coatings in gas turbine engine applications," *Journal of Engineering for Gas Turbines and Power*, vol. 116, no. 1, pp. 250–257, 1994.

[9] R. A. Miller, "Life modeling of thermal barrier coatings for aircraft gas turbine engines," in *Towards Improved Durability in Advanced Aircraft Engine Hot Sections*, D. E. Sokolowski, Ed., NASA TM4087, 1989.

[10] S. M. Meier, D. M. Nissley, and K. D. Sheffler, "Thermal barrier coating life prediction model development," Phase II Final Report Contract NAS3-23944, NASA CR, 189111, 1991.

[11] S. Bose and J. Masi-Marsin, "Thermal barrier coating experience in gas turbine engines at pratt and whitney," in *Proceedings of the Thermal Barrier Coating Workshop*, p. 63, NASA, 1995.

[12] W. Tabakoff and T. Wakeman, "Test facility for material erosion at high temperature," *ASTM Special Publication*, vol. 664, pp. 123–135, 1979.

[13] W. Tabakoff, "Investigation of coatings at high temperature for use in turbomachinery," *Surface and Coatings Technology*, vol. 940, pp. 97–115, 1989.

[14] J. R. Nicholls, M. J. Deakin, and D. S. Rickerby, "A comparison between the erosion behaviour of thermal spray and electron beam physical vapour deposition thermal barrier coatings," *Wear*, vol. 233–235, pp. 352–361, 1999.

[15] M. F. Hussein and W. Tabakoff, "Dynamic behavior of solid particles suspended by polluted air flow in a turbine stage," *Journal of Aircraft*, vol. 107, pp. 434–440, 1973.

[16] A. A. Hamed, W. Tabakoff, R. B. Rivir, K. Das, and P. Arora, "Turbine blade surface deterioration by erosion," *Journal of Turbomachinery*, vol. 127, no. 3, pp. 445–452, 2005.

[17] A. Hamed and W. Tabakoff, "Experimental and numerical simulations of the effects of ingested particles in gas turbine engines," Tech. Rep. AGARD-CP-558, Erosion, Corrosion and Foreign Object Effects in Gas Turbines, 1994.

[18] W. Tabakoff, A. Hamed, and B. Beacher, "Investigation of gas particle flow in an erosion wind tunnel," *Wear*, vol. 86, no. 1, pp. 73–88, 1983.

[19] J. A. Gunaraj, W. Tabakoff, and S. Siravuri, "Experimental investigation of solid particles interaction in particulate flow," in *Proceedings of the ASME Fluids Engineering Division Summer Meeting*, June 1997.

[20] J. A. Gunaraj, *Study of the effect particle-particle interactions in the particulate flow [Ph.D. thesis]*, University of Cincinnati, 1997.

[21] S. Shastri, *Particle rebound characteristics of turbomachinery cascade leading edge geometry [Ph.D. thesis]*, University of Cincinnati, 1999.

[22] ANSYS CFX, Release 12. 1, User Manual, 2009.

[23] Pointwise, Release 16. 04, User Manual, 2011.